A WAVE SPLITTING/INVARIANT EMBEDDING APPROACH TO AN ULTRASONIC INVERSE PROBLEM

Paul Stucky
Electrical and Computer Engineering
Iowa State University
Ames, Iowa 50011

William Lord
Electrical and Computer Engineering
Iowa State University
Ames, Iowa 50011

INTRODUCTION

Material property measurement is an important area of basic and applied research and can be defined as an inverse problem in which knowledge of the system input and output can be used to determine material properties.

A tool for studying the forward and inverse problems, denoted here as wave splitting and invariant embedding (WSIE), has been developed and offers unique physical insights [1] [2] [3]. Wave splitting and invariant embedding (WSIE) is a theory which relates material properties to system *impulse response functions* in precise ways. WSIE theory provides a clear way for solving the inverse problem if the response functions are known. In turn impulse response functions relate system inputs to the outputs. If response functions can be recovered from measured system inputs and outputs then WSIE has potential application for determining material properties.

Recent experiments in an electromagnetic coaxial line system utilizing wave splitting and invariant embedding signal processing techniques have demonstrated the proof of principle of material property reconstruction for linear, isotropic and spatially inhomogeneous dielectric material [4] as well as for LHI dispersive material [5]. The mechanical analog to electromagnetic LHI dispersive media is LHI viscoelastic media. Most polymeric solids and liquids can be described by linear viscoelasticity theory under conditions of infinitesimal stress, strain and displacement [6]. Considering the success of these two experiments employing electromagnetic waves, the question is posed: 'can the viscoelastic moduli of an LHI viscoelastic medium be reconstructed from knowledge of the incident, reflected and transmitted ultrasonic waves using wave splitting and invariant embedding techniques?'

WAVE SPLITTING AND INVARIANT EMBEDDING

Ultrasonic wave propagation through LHI viscoelastic has been previously discussed in the context of time-domain finite element modeling [7] [8] [9]. For one dimensional wave propagation the appropriate wave equations for longitudinal displacement in terms of a stress relaxation modulus or, equivalently, a creep compliance are, respectively, [10]:

$$\frac{1}{c^2}\ddot{u}_z(z,t) = \partial_z^2 u_z(z,t) + \dot{m} * \partial_z^2 u_z(z,t) \tag{1}$$

$$\partial_z^2 u_z(z,t) = \frac{1}{c^2}\ddot{u}_z(z,t) + \frac{1}{c^2}\dot{n} * \ddot{u}_z(z,t) \tag{2}$$

where the normalized longitudinal stress relaxation modulus, $m(t)$, creep compliance, $n(t)$, and the wave speed, c, are defined by

$$m(t) = \frac{M(t)}{M(0)} \tag{3}$$

$$n(t) = \frac{N(t)}{N(0)} \tag{4}$$

$$c = \sqrt{\frac{M(0)}{\rho}} = \frac{1}{\sqrt{\rho N(0)}}. \tag{5}$$

Review of Progress in Quantitative Nondestructive Evaluation, Vol. 16
Edited by D.O. Thompson and D.E. Chimenti, Plenum Press, New York, 1997

The relationship between the creep compliance and the stress relaxation modulus is [6]

$$[n * m](t) = t. \tag{6}$$

The wave splitting and invariant embedding formulation for one spatial dimension has previously been described in detail elsewhere [11] [12]. The main points are repeated here with only slight modification in some definitions. The longitudinal stress/displacement relationship in one dimension in terms of $m(t)$ or $n(t)$ is given by (dropping subscripts)

$$\begin{aligned} T(z,t) &= m * \partial_z \dot{u}(z,t) && (7)\\ \partial_z u(z,t) &= n * \dot{T}(z,t) && (8)\\ &= [1 + \dot{n}*]T(z,t). && (9) \end{aligned}$$

The wave equation becomes

$$\partial_z T(z,t) = \frac{1}{c^2}\ddot{u}(z,t). \tag{10}$$

or as first order system

$$\partial_z \begin{bmatrix} u \\ T \end{bmatrix} = \left\{ \begin{bmatrix} 0 & 1 \\ \left(\frac{\partial_t}{c}\right)^2 & 0 \end{bmatrix} + \begin{bmatrix} 0 & \dot{n}* \\ 0 & 0 \end{bmatrix} \right\} \begin{bmatrix} u \\ T \end{bmatrix} = (\underline{A} + \underline{B}) \begin{bmatrix} u \\ T \end{bmatrix}. \tag{11}$$

The wave splitting is a change of basis from total displacement and stress, (u,T), to total displacement propagating in the plus and minus z-direction, (u^+,u^-), respectively. The system matrix, $\underline{A}$, is diagonalized by a similarity transformation [3]

$$\underline{D} = \underline{P}\,\underline{A}\,\underline{P}^{-1} = \begin{bmatrix} -\left(\frac{\partial_t}{c}\right) & 0 \\ 0 & \left(\frac{\partial_t}{c}\right) \end{bmatrix} \tag{12}$$

where $\underline{D}$ is the matrix of eigenvalues of $\underline{A}$ and $\underline{P}^{-1}$ is recognized to be the matrix of eigenvectors of $\underline{A}$. The matrices $\underline{P}^{-1}$ and $\underline{P}$ relate (u,T) and (u^+,u^-) by

$$\begin{bmatrix} u \\ T \end{bmatrix} = \begin{bmatrix} 1 & 1 \\ -\left(\frac{\partial_t}{c}\right) & \left(\frac{\partial_t}{c}\right) \end{bmatrix} \begin{bmatrix} u^+ \\ u^- \end{bmatrix} = \underline{P}^{-1} \begin{bmatrix} u^+ \\ u^- \end{bmatrix} \tag{13}$$

$$\begin{bmatrix} u^+ \\ u^- \end{bmatrix} = \frac{1}{2} \begin{bmatrix} 1 & -\left(\frac{\partial_t}{c}\right)^{-1} \\ 1 & \left(\frac{\partial_t}{c}\right)^{-1} \end{bmatrix} \begin{bmatrix} u \\ T \end{bmatrix} = \underline{P} \begin{bmatrix} u \\ T \end{bmatrix} \tag{14}$$

where

$$\left[\left(\frac{\partial_t}{c}\right)^{-1} f\right](t) \equiv c \int_0^t f(s)ds, \tag{15}$$

assuming initial conditions for all field variables are zero [3]. The similarity transformation of the matrix, $\underline{B}$, gives

$$\underline{E} = \underline{P}\,\underline{B}\,\underline{P}^{-1} = \frac{1}{2c} \begin{bmatrix} -\dot{n} * \partial_t & \dot{n} * \partial_t \\ -\dot{n} * \partial_t & \dot{n} * \partial_t \end{bmatrix}. \tag{16}$$

Collecting these results together, an equivalent formulation of the wave equation results:

$$\partial_z \begin{bmatrix} u^+ \\ u^- \end{bmatrix} = \begin{bmatrix} \alpha & \beta \\ \gamma & \delta \end{bmatrix} \begin{bmatrix} u^+ \\ u^- \end{bmatrix} \tag{17}$$

where

$$\delta = -\alpha = \frac{1}{2c}[2 + \dot{n}*]\,\partial_t \tag{18}$$

$$\beta = -\gamma = \frac{1}{2c}\dot{n} * \partial_t. \tag{19}$$

With this reformulation of wave propagation in LHI viscoelastic media, the wave splitting is complete.

To introduce invariant embedding consider the scattering problem depicted in fig. 1. Assume the source extends to infinity in the radial direction and emits plane waves. A viscoelastic slab is sandwiched between two elastic halfspaces. Assume the elastic halfspaces and the viscoelastic slab are impedance matched, that is,

$$Z_e = [\rho c]_{\text{elastic}} = [\rho c]_{\text{viscoelastic}} = Z_{ve}. \tag{20}$$

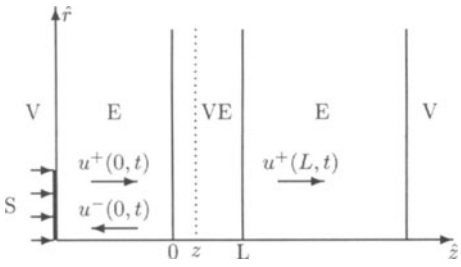

Figure 1: Geometry of the test problem, V, E, VE, S imply vacuum, elastic, viscoelastic and source, respectively

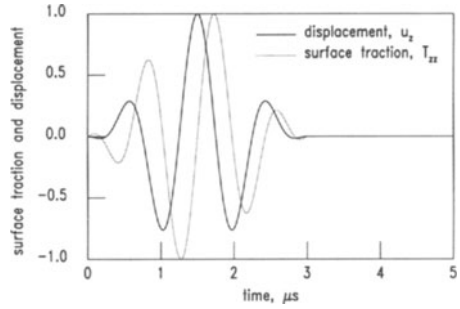

Figure 2: Time dependence of the surface traction and displacement, normalized, $f_0 = 1$MHz

The desired result is a precise relationship between the material properties and the impulse response functions for the slab of thickness L. Invariant embedding provides a mechanism by which this can be accomplished. The problem of finding the impulse response function/material property relationship for the slab of thickness L is embedded in a more general problem of finding the impulse response functions for a slab of thickness $L - z$, that is, the left most boundary of the slab is allowed to vary. This statement is equivalent to asking how the impulse response functions of a slab from $a < z < L$ change if a very thin layer of similar material of thickness Δz is added to the original slab at the boundary a so that now the slab extends from $a - \Delta z < a < z < L$. The details of the derivation based on this idea can be found in Davison [3] in the context of one-dimensional spatially inhomogeneous medium. The results for viscoelastic media based on the invariant embedding method are presented in Ammicht [11] and Karlsson [12]. For interest in invariant embedding methods in general see Bellman and Wing [13].

Since the system is assumed linear and time translation invariant, there exist linear operators that map the incident displacement, $u^+(z,t)$, onto the reflected displacement, $u^-(z,t)$, and the transmitted displacement, $u^+(L, t + \tau(z)/2)$, where $\tau(z) = 2(L - z)/c$ is the round-trip time for a wave to traverse the viscoelastic slab from z to L and back or vice versa. The operators for the impedance matched case have the following explicit representations [12]:

$$u^-(z,t) = \left[\mathcal{R}u^+\right](z,t) \tag{21}$$

$$= \left[R * u^+\right](z,t) \tag{22}$$

$$u^+(L, t+\tau(z)/2) = \left[\mathcal{T}u^+\right](z,t) \tag{23}$$

$$= d(z)u^+(z,t) + \left[T * u^+\right](z,t) \tag{24}$$

where $\mathcal{R}$, $\mathcal{T}$, and $R(z,L,t)$, $T(z,L,t)$, are the reflection and transmission operators and kernels, respectively. The term, $d(z)$, represents the attenuation of the directly transmitted incident wave,

$$d(z) = e^{-n(0)\tau(z)/4}. \tag{25}$$

Using the definition of the transmission and reflection operators, eqns. 22 and 24, and the wave splitting, eqn. 17, it has been shown [11] [12] that for an arbitrary incident field the impedance-matched transmission and reflection kernels satisfy first order partial integro-differential equations in time and space. The resulting equations give explicit and mathematically well-posed relations between the reflection and transmission kernels (impulse response functions) and the dispersive material properties. These equations can be solved numerically for the forward and inverse problems with impedance mismatched front and back walls. In the forward problem the material properties are known and the reflection and transmission kernels are computed, whereas in the inverse problem the reflection and transmission kernels are known and the material properties are determined.

It has been shown by Fuks [5] in an analogous paper for dispersive electromagnetic media that the reflection and transmission kernels are related to dispersive material properties by time-domain Volterra integral equations of the second kind independent of space due to spatial homogeneity of the medium. Although both approaches are analogous, it is the method of Fuks which is adopted here due to its simplicity and reduced computation time. For viscoelastic media the appropriate equations for the reflection and transmission kernels with impedance matched front and back walls are

$$R(t) = r(t) + \sum_{i=0}^{\infty} S((i+1)\tau(0)) \left[(r * r * v - v)(*r * v)^i\right](t) \tag{26}$$

$$T(t) = e(t) - d(0)\,[r * R]\,(t) - [e * r * R]\,(t) \tag{27}$$

where

$$r(t) = \frac{1}{4}\left(\dot{n}(t) - 2\,[\dot{n} * r]\,(t) + [\dot{n} * r * r]\,(t)\right) \tag{28}$$

$$v(t) = d^2(0)r(t) + 2d(0)\,[r * e]\,(t) + [r * e * e]\,(t) \tag{29}$$

$$e(t) = -\frac{1}{2t}\,[(tb) * e]\,(t) - \frac{1}{2}d(0)b(t) \tag{30}$$

$$b(t) = \frac{\tau(0)}{2c}\left(\ddot{n}(t) - \dot{n}(0)r(t) - [\dot{n} * r]\,(t)\right). \tag{31}$$

The terms $r(t)$, $R(t)$ and $T(t)$ are the reflection kernel for an impedance-matched viscoelastic halfspace and slab and the transmission kernel for the slab, respectively. Dependence on the length of the slab, L, has been implicitly assumed in eqns. 26 through 31. The term $S(\tau(0))$ is defined to be the time translation operator,

$$[S(\tau(0))f]\,(t) \equiv f(t - \tau(0)). \tag{32}$$

Equations 26 through 31 are derived from Laplace domain expressions for the reflection and transmission kernels for a viscoelastic slab defined from $0 \leq z \leq L$. For details and the reflection and transmission kernel equations for impedance mismatched front and back walls please see [12], see also [5].

NUMERICAL EXPERIMENT DESCRIPTION

An initial numerical experiment to test the effect of band-limiting and edge waves[1] on modulus reconstruction utilizes a finite element program capable of quantitatively modelling ultrasonic wave propagation in elastic and viscoelastic media [7]. The geometry consists of a 4mm thick viscoelastic slab sandwiched between two elastic slabs. The viscoelastic slab is assumed impedance-matched to the elastic slabs, see geometry in fig. 1. The longitudinal stress relaxation modulus is assumed to have the following simple form:

$$M(t) = \left[M_e + (M_g - M_e)e^{-t/\tau}\right] H(t) \tag{33}$$

where $M_g = M(0)$, $M_e = M(t \to \infty)$, $\tau = 0.1\mu s$ and $H(t)$ is the Heaviside step function. The subscripts "g" and "e" imply glassy or elastic and equilibrium or low frequency modulus, respectively, with $M_e < M_g$. The shear stress relaxation modulus has the same form as eqn. 33 but with G replacing M. The values used in the numerical calculations are the following:

$$M_g = \rho c^2 = 107.2 \text{ GPa} \tag{34}$$

$$M_e = \rho c_e^2 = 26.8 \text{ GPa} \tag{35}$$

$$G_g = \rho c_s^2 = 25.9 \text{ GPa} \tag{36}$$

$$G_e = \rho c_{se}^2 = 0 \text{ GPa} \tag{37}$$

where $\rho = 2700kg/m^3$, $c = 6300m/s$, $c_e = 3150m/s$, $c_s = 3100m/s$ and $c_{se} = 0m/s$ (subscript s stands for shear). The distance from the source to the viscoelastic slab front surface was varied in proportion to the wavelength of the source at center frequency. This was necessary to remove effects of re-reflections off the vacuum/elastic surface.

A variable aperture source is placed on the vacuum/elastic interface, see fig. 1. The time dependence of the surface traction is defined by the time derivative of the desired input displacement (source function), see fig. 2:

$$u_z(r,0,t) = \begin{cases} -\frac{1}{2}\left[1 - \cos(\frac{\omega_0}{3}t)\right]\cos(\omega_0 t) & 0 \leq \omega_0 t \leq 6\pi;\ \ r \leq a \\ 0 & \text{otherwise} \end{cases} \tag{38}$$

$$T_{zz}(r,0,t) = \begin{cases} -Z_l \dot{u}_z & 0 \leq \omega_0 t \leq 6\pi;\ \ r \leq a \\ 0 & \text{otherwise} \end{cases} \tag{39}$$

where $Z = \rho c$ is the longitudinal mechanical impedance of the elastic medium and the aperture radius is denoted by "a".

The frequency spectrum magnitude of the longitudinal modulus is plotted in fig. 3 against the spectrum magnitude of the source function for three different center frequencies, 100kHz, 1MHz and 5MHz. It is clear that the available bandwidth of the source is not great enough to resolve the

[1] Edge waves, both longitudinal and shear, are produced at the rim of a piston source and decay with distance due to geometrical spreading.

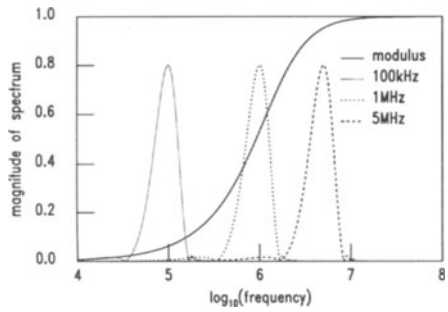

Figure 3: Frequency spectrum magnitude of incident waves and relaxation modulus, normalized

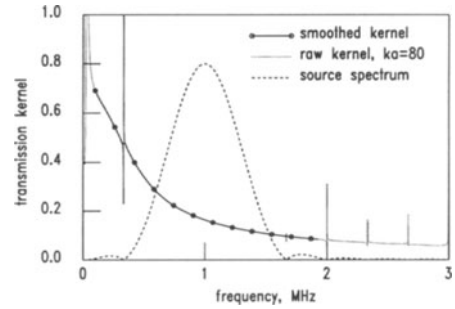

Figure 4: Deconvolved transmission kernel magnitude, raw and smoothed, versus the incident wave source spectrum

complete modulus spectrum, therefore, numerical results obtained at each frequency must be combined. For each frequency the radius of the source is varied and data at each frequency are combined for similar ka, where $k = 2\pi/\lambda$ is the wave number and λ is the wavelength of the longitudinal wave in the elastic medium corresponding to the center frequency of the source. For the results presented, $5 \leq ka \leq 80$ where $ka = 80$ approximates plane wave conditions. Almost without exception realistic viscoelastic materials have much broader spectrums than the single exponential spectrum, hence data must be combined from more than one experiment to form a complete modulus spectrum [6].

Frequency domain deconvolution was applied to the incident and transmitted waves to recover the transmission kernel. No special frequency domain filters were used. For the impedance matched case the transmission kernel, eqn. 24, becomes

$$T(\omega) = \frac{u^+(L,\omega)}{u^+(0,\omega)} - d(0) \tag{40}$$

where $d(0)$ is the attenuation of the directly transmitted incident field for $0 \leq z \leq L$. The value of $d(0)$ was found by comparing the peak magnitude of a transmitted wave with the incident wave at a center frequency of 10MHz. At this frequency the transmission kernel is small and the major contribution to the attenuation is from $d(0)$. By this method $d(0) \approx 0.0917$ while the true value is $d(0) = 0.0925$. Before deconvolution the propagation delay for the wave to traverse the viscoelastic slab, $\tau(0)/2$, was removed from the transmitted wave. This amounts to knowing the wave speed, c, of the slab which is *a priori* information. Questions concerning *a priori* information will be addressed in future work.

The band-limiting nature of the source function required creating a composite frequency domain kernel from data obtained at three frequencies. A simple smoothing and truncating procedure is used and is depicted in fig. 4 for $ka = 80$. Only deconvolution results from the main lobe and portions of the first side lobes in the source spectrum at each frequency were used. At the points where the source spectrum goes to go zero a simple linear fit was made using data from just above and just below this frequency. The inverse algorithm which uses the recovered time-domain transmission kernel to reconstruct the derivative of the creep compliance is described in detail elsewhere and is not repeated here [12] [5].

RESULTS

Axisymmetric finite element results showing the displacement incident on and transmitted through the viscoelastic slab for various ka and $f_0 = 1$MHz are shown in figs. 5 and 6 with similar results for 100kHz and 5MHz. The incident wave is obtained by replacing the viscoelastic slab with an elastic slab and recording the wave as it passes the point along the axis of symmetry corresponding to the front surface of the slab. From an experimental point of view this is impractical but is valid in a numerical study since it allows isolation and study of separate effects. The transmitted wave is recorded at the viscoelastic slab back face as the wave passes out of the slab.

The longitudinal edge wave is clearly apparent in fig. 5(a) following the plane wave component. The edge wave emanates from the edge or rim of the source and decays with distance due to geometrical spreading. As the radius is reduced the delay between the tail of the plane wave component and the head of the longitudinal edge wave is also reduced. From the point of view of the one dimensional modulus reconstruction algorithm the edge waves represent a systematic error introduced into the plane wave transmission kernel.

For large enough ka the edge wave can be filtered (windowed) out, but as the radius decreases the edge wave and the plane wave become coincident and unseparable. The coincidence is

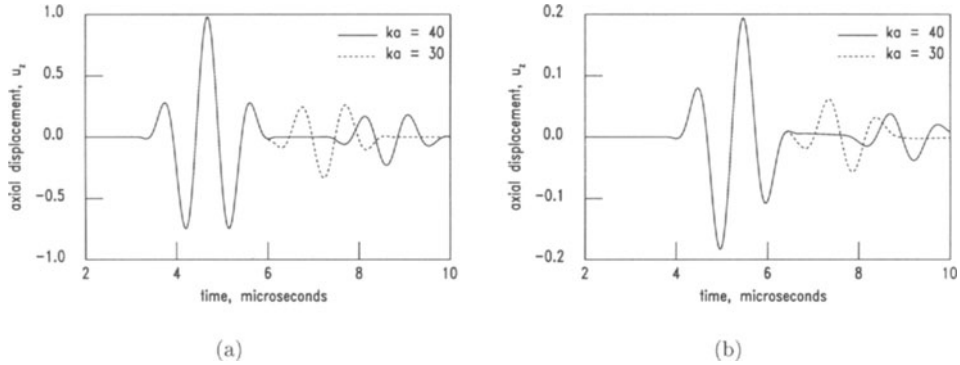

Figure 5: Incident (a) and transmitted (b) axial displacement at $(r, z) = (0, 2)$cm and $(r, z) = (0, 2.4)$cm, respectively, at $f_0 = 1$MHz showing effect of the longitudinal edge wave for decreasing aperture radius

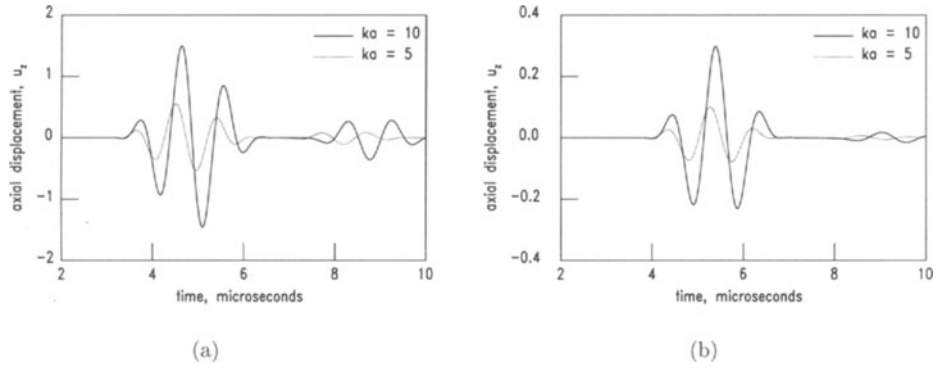

Figure 6: Incident (a) and transmitted (b) axial displacement at $(r, z) = (0, 2)$cm and $(r, z) = (0, 2.4)$cm, respectively, at $f_0 = 1$MHz showing effect of the longitudinal edge wave for decreasing aperture radius

demonstrated in fig. 6 where the longitudinal edge wave is indistinguishable from the plane wave. Notice that for $ka = 10$ the peak magnitude of the main signal has increased beyond one while the peak has decreased to approximately one half of one for $ka = 5$. Clearly, the edge wave has perturbed the otherwise plane wave portion of the field in front of the piston source and the effect on the modulus reconstruction is important to understand. The shear edge waves can be seen in fig. 6 following the main signal.

The composite frequency domain transmission kernel for various ka is shown in figs. 7(a) and 8(a) and the corresponding time domain kernels in figs. 7(b) and 8(b). As is expected, when $ka = 80$ the composite kernel most closely approximates the true kernel. For $ka = 30$ the inclusion of the edge wave results in a pronounced oscillation about the true kernel although the general trend is preserved suggesting that for the given geometry the viscoelastic effects have a greater influence on the kernel. In fact, in fig. 8(a) where $ka = 5$ and 10 the edge wave effects have diminished, especially for increasing frequency. Comparing the time domain kernels in figs. 7(b) and 8(b) with the true curve shows that truncation of high frequencies (< 10MHz) results in loss of resolution at short times ($< 1\mu$s) which is expected, whereas the edge wave for $ka = 30$ contributes large variations about the true value for $t \leq 3\mu s$.

The function directly reconstructed in the inverse algorithm is the derivative of the normalized creep compliance, $\dot{n}(t)$. The reconstruction for three values of ka are shown in fig. 9(a). Even with large oscillations in the recovered transmission kernel the reconstructions have the basic trend of the true curve. The normalized stress relaxation modulus shown in fig. 9(b) is obtained first by integrating $\dot{n}(t)$ to obtain the creep compliance then solving eqn. 6 to get $m(t)$. Integration naturally smooths the oscillations. The modulus deviates from the true curve at longer times for decreasing ka. Qualitatively, the long-time response is related to the quality of the low frequency information recovered in the numerical experiment. In the examples presented the transmission kernel has much of its structure in the region $f \leq 2$MHz, therefore a highly degraded kernel in this region will potentially cause severe distortion in the reconstructed modulus.

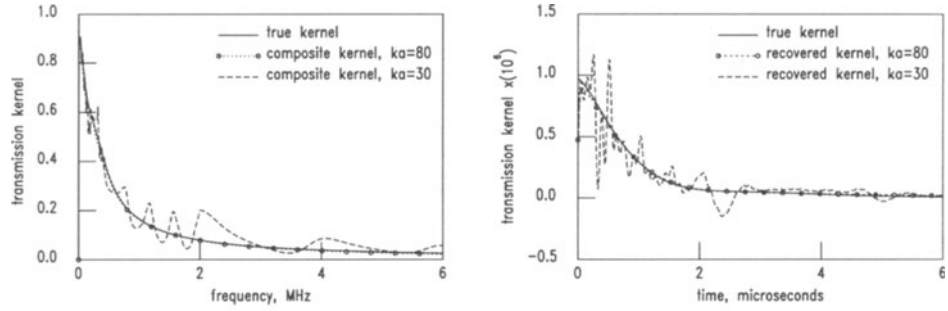

(a) (b)

Figure 7: Deconvolved and smoothed transmission kernel versus true kernel magnitude showing the effect of edge waves on the recovered kernel, frequency (a) and time (b) domain

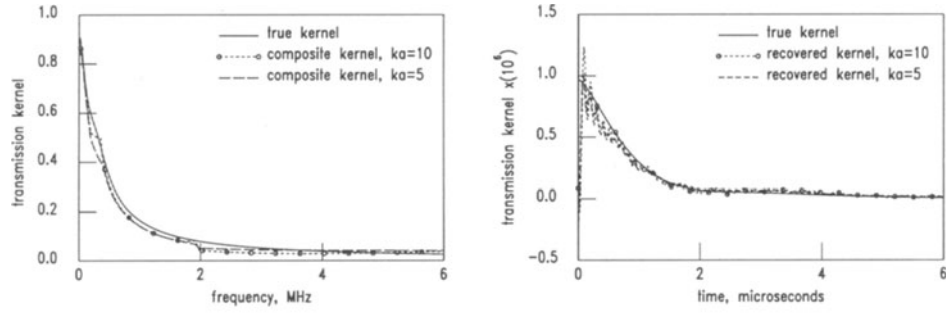

(a) (b)

Figure 8: Deconvolved and smoothed transmission kernel versus true kernel showing the diminished effect of edge waves for decreasing ka, frequency (a) and time (b) domain

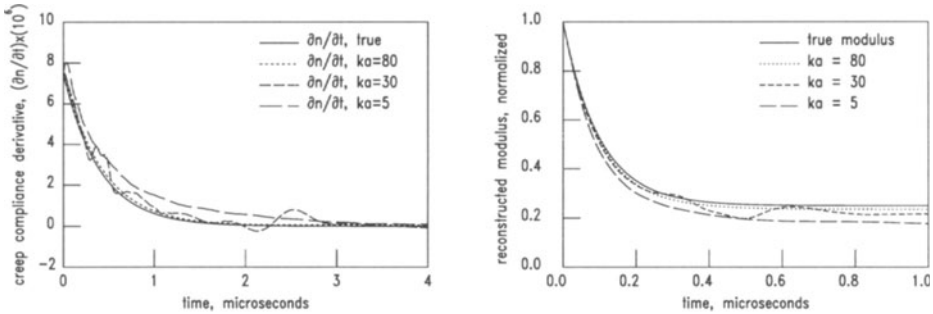

(a) (b)

Figure 9: Reconstructed derivative of the creep compliance, $\dot{n}(t)$, (a), and relaxation modulus, $m(t)$, (b), for various ka compared with the true curves

CONCLUDING REMARKS

The purpose of this initial investigation is to demonstrate what effects non-planar edge waves have on reconstructions of viscoelastic material properties when using plane wave based WSIE inverse methods. A very simple exponential viscoelastic model was employed. The transient wave data was produced using a finite element wave propagation program modified to model viscoelastic and elastic media simultaneously. With a large source aperture plane wave conditions were achieved. In this case modulus reconstruction was closest to the exact modulus and demonstrated the validity of the inverse method, at least in principle. It was shown that including longitudinal edge waves with plane waves during recovery of the transmission kernel does degrade the kernel by creating oscillations in the reconstructed modulus. The oscillations increase and then decrease as the radius decreases and the plane wave and edge wave become coincident. This result was not expected and demonstrates the inverse method's robustness in the presence of finite apertures. It may also suggest that standard diffraction corrections may be enough to correct for excess attenuation due to geometrical spreading of the wave. Future work will model more realistic experimental conditions including typical viscoelastic material properties, wave sources, detection schemes and experimental geometries to determine a feasible experimental method.

ACKNOWLEDGEMENTS

I wish to thank Dr. James Corones and Applied Mathematical Sciences of Ames Laboratory, Ames, Iowa, for financial support during this project as well as access to excellent computer resources and office space.

REFERENCES

1. James P. Corones, Mark E. Davison, Robert J. Krueger, "Wave splittings, invariant embedding and inverse scattering," *Inverse Optics, Proceedings of SPIE,* vol. 413, pp.102-6.

2. James P. Corones, Mark E. Davison, Robert J. Krueger, "Direct and inverse scattering in the time domain via invariant embedding equations," *J. Acoust. Soc. Am.* vol. 74, p1535-41, 1983.

3. Mark E. Davison, Ronald C. Winther, "A general approach to splitting and invariant imbedding for linear wave equations," *J. Math. Anal. Appl.,* vol. 188 no. 1, pp.158-81, Nov. 15, 1994.

4. Peter Fuks, Gerhard Kristensson, Gunnar Larson, "Permittivity profile reconstructions using transient electromagnetic reflection data," Technical Report CODEN:LUTEDX/(TEAT-7009)/ 1990, pp1-88, Dept. of Electromagnetic Theory, Lund Institute of Technology, Lund, Sweden.

5. Peter Fuks, Anders Karlsson, Gunnar Larson, "Direct and inverse scattering from dispersive media," *Inverse Problems,* vol. 10 pp.555-71, 1994.

6. John D. Ferry, *Viscoelastic Properties of Polymers,* 3rd ed., John Wiley and Sons, Inc., New York, 1980.

7. Paul Stucky, William Lord, "Finite element modeling of ultrasonic waves in viscoelastic media," these proceedings, QNDE 96.

8. You, Z., Lusk, M., Ludwig, R., Lord, W., "Numerical simulation of ultrasonic wave propagation in anisotropic and attenuative solid materials," *IEEE Trans. UFFC,* 38(5), Sept. 1991, pp436-45.

9. Xue, T., Lord, W., Udpa, S., "Transient fields of pulsed transducers in solids," *Res. Nondestr. Eval.,* 7, 1995, pp31-53.

10. Jean-Paul Charlier, Françoise Crowet, "Wave equations in linear viscoelastic materials," *J. Acoust. Soc. Am.,* vol. 79, no. 4, pp.895-900, April 1986.

11. E. Ammicht, J. P. Corones, R. J. Krueger, "Direct and inverse scattering for viscoelastic media," *J. Acoust. Soc. Am.,* vol. 81, no. 4, pp. 827-34, April 1987.

12. Anders Karlsson, "Inverse scattering for viscoelastic media using transmission data," *Inverse Problems,* vol. 3, pp. 691-709, 1987.

13. Richard Bellman, Milton Wing, *An Introduction to Invariant Embedding,* SIAM, Philadelphia, 1992.